Effect of natural convection in a horizontally oriented cylinder on NMR imaging of the distribution of diffusivity

Aleš Mohorič
Physics Department, Faculty of Mathematics and Physics, University of Ljubljana, Jadranska 19, 1000 Ljubljana, Slovenia

Janez Stepišnik
Physics Department, Faculty of Mathematics and Physics, University of Ljubljana, Jadranska 19, 1000 Ljubljana, Slovenia and Institute Josef Stefan, Jamova 39, 1000 Ljubljana, Slovenia

(Received 23 July 1999)

This paper describes the influence of natural convection on NMR measurement of a self-diffusion constant of fluid in the earth's magnetic field. To get an estimation of the effect, the Lorenz model of natural convection in a horizontally oriented cylinder, heated from below, is derived. Since the Lorenz model of natural convection is derived for the free boundary condition, its validity is of a limited value for the natural no-slip boundary condition. We point out that even a slight temperature gradient can cause significant misinterpretation of measurements. The chaotic nature of convection enhances the apparent self-diffusion constant of the liquid.

PACS number(s): 44.25.+f, 47.27.Te, 92.60.Ek, 87.61.−c

I. INTRODUCTION

Nuclear magnetic resonance (NMR) pulsed-gradient spin echo (PGSE) has long been used to investigate correlated and uncorrelated motion in a number of systems. The effects of self-diffusion on the NMR signal of liquids have been known since the beginnings of NMR (Refs. [1–6]) and since then, spin-echo measurement of a self-diffusion constant has been a common practice ([7,1]) and also extensively used in our lab [8]. Some experiments where diffusivity measurement has been combined with magnetic resonance imaging (MRI) to study the distribution of diffusivity have also been performed [9–11]. The effect of natural convection on the measurements is well-known [12,13] and improvements of measurements have been proposed [14,15]. Natural convection has recently been investigated with magnetic resonance imaging [16,17].

In the following paper, natural convection inside a horizontally oriented cylinder, heated from below, is inspected and its effect is evaluated. Natural convection has been thoroughly studied in certain geometries such as plane geometry [18–20] and vertically oriented cylinder [21,22]. Horizontally oriented cylinder is used as a probe for measurements of self-diffusion constant distribution in the earth's magnetic field on a homemade device as described in [8,10].

First we describe the signal of a PGSE experiment. Then we simplify fluid-dynamics equations to get the Lorenz model [23] of convection. The derivation closely follows Saltzman's procedure [24] for plane geometry. The natural no-slip boundary condition is not fully regarded and the resulting model is only an approximation of the system. Since the boundary temperature is not controlled, the resulting model is approximate. It only serves as a tool to estimate the order of the temperature gradient and velocity fluctuations. In the last section, we show the experimental results and evaluate the conditions and the effect.

II. NMR SPIN ECHO

With the spin echo NMR, a nonuniform magnetic field (magnetic field gradient) is used to encode the magnetization for motion by refocusing any spin phase shift of nonmoving spins. The change of the signal phase at the time of the spin echo τ due to the molecular displacements in the effective magnetic field gradient $\mathbf{G}(\mathbf{r},t)$ for a spin j, whose trajectory is given with $\mathbf{r}_j(t)$, is $\Phi(\mathbf{r}_j,\tau) = \gamma\int_0^\tau \mathbf{G}(\mathbf{r}_j,t)\cdot\mathbf{r}_j(t)dt = \int_0^\tau \mathbf{F}(\mathbf{r},t)\cdot\mathbf{v}_j(\mathbf{r},t)dt$. Here $\mathbf{F}(\mathbf{r},t) = \gamma\int_0^t \mathbf{G}(\mathbf{r},t')dt'$ is zero at the time of refocusing τ. $\mathbf{v}_j$ is the velocity of the spin-bearing particle. The magnetic field gradient can be written as $\mathbf{G}(\mathbf{r},t) = g_t(t)\mathbf{g}_r(\mathbf{r})$. The scalar function g_t describes the gradient time variation and the vector function $\mathbf{g}_r$, its spatial dependence $\nabla|B(\mathbf{r})|$. The word effective signifies the change in sign of g_t whenever a π rf pulse is applied to the system. The effective time dependence g_t of the gradient field for a typical PGSE experiment is shown in Fig. 1. Since the detected signal arises from the induction of an immense number of spins ($\gg 10^6$), one does not detect the frequency fluctuations of an individual spin but rather a coherent superposition of signals induced by a large number of spins. The detected spin-echo signal of a picture element positioned at $\mathbf{r}$ in an MR image can be written as

$$E(\mathbf{r},\tau) = \sum_j e^{i\Phi(\mathbf{r}_j,\tau)} = n\langle e^{i\Phi(\mathbf{r},\tau)}\rangle = E_0 e^{i\phi(\mathbf{r})-\beta(\mathbf{r})}, \quad (1)$$

where the sum encloses the n spins of the fluid parcel within

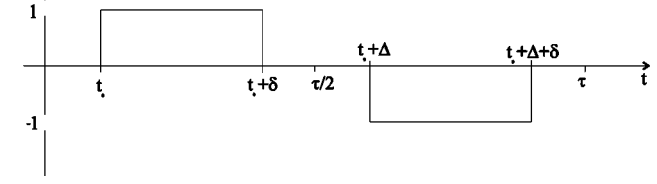

FIG. 1. The time dependence $g_t(t)$ of the magnetic field gradient in a typical PGSE experiment. The gradient pulses are δ long and Δ apart. Spin-echo forms at time τ.

the picture element. The sum can be evaluated with an ensemble average $\langle \cdots \rangle$ over the trajectories of different spins contributing to the picture element. E_0 is the normalized amplitude. The phase shift due to the net flow is

$$\phi(\mathbf{r},\tau)=\int_0^\tau \mathbf{F}(\mathbf{r},t)\cdot\langle \mathbf{v}(\mathbf{r},t)\rangle dt, \tag{2}$$

while the signal attenuation is

$$\beta(\mathbf{r},\tau)=\int_0^\tau\int_0^\tau \mathbf{F}(\mathbf{r},t_1)\cdot\langle \partial\mathbf{v}(\mathbf{r},t_1)\partial\mathbf{v}(\mathbf{r},t_2)\rangle\mathbf{F}(\mathbf{r},t_2)dt_1dt_2, \tag{3}$$

if the velocity fluctuation $\partial\mathbf{v}=\mathbf{v}-\langle\mathbf{v}\rangle$ is considered a variable of the Gaussian stochastic process. This allows the truncation of the cumulant expansion to the second order when used for the phase averaging [8]. Therefore the process is defined only by the variance $\langle\partial\mathbf{v}(t)\partial\mathbf{v}(0)\rangle$, i.e., the velocity correlation function. In the case of the molecular thermal motion an immense number of spins, each experiencing weak phase fluctuations, adds to the induction in the detection coil. This assures that the spin-echo phase fluctuation can be treated as a Gaussian process. But for the velocity variation of a nonstationary or turbulent flow, the associated spin phase fluctuations may in general not justify the truncation of higher terms in the cumulant expansion. With an appropriate selection of timing and intervals of the signal acquisition with respect to the speed and pace of the flow, one can enhance the Gaussian assumption to allow the use of Eq. (3) for the flow fluctuation as well. Namely, in the case of thermal convection, slow flow $\mathbf{v}_C$ is superposed on fast molecular Brownian motion $\mathbf{v}_m$. The average velocity of Brownian motion is $\langle\mathbf{v}_m\rangle=0$ and this motion does not contribute to the phase ϕ of the signal. Almost stationary flow $\mathbf{v}_C$ effects only the signal phase but not the amplitude in Eq. (1) during the short interval of motion encoding and echo acquisition. With the NMR in the earth's magnetic field, the signal averaging for noise reduction is performed. The duration of each gradient sequence τ is limited by the spin relaxation and can rarely be longer than a few seconds. Thus a change of the convection flow velocity $\mathbf{v}_C$, that can occur within each signal acquisition, is small but the velocity can be different for every frame of acquisition and so can the phase shifts ϕ. Subsequent addition of different frames, needed to reduce the noise, weakens the signal from every parcel of fluid and thus the intensity of a corresponding picture element by a factor $e^{-\beta_C}$, where

$$\beta_C(\mathbf{r})=\frac{1}{2N}\sum_{n=1}^{N}\left(\phi_n^2(\mathbf{r})-\frac{1}{N}\sum_{m=1}^{N}\phi_m(\mathbf{r})\phi_n(\mathbf{r})\right). \tag{4}$$

Here N is the number of frames added in the averaging process, and ϕ_n is the phase accumulated in the nth frame. In the limit of many accumulations, β_C gets the form of Eq. (3), where the velocity variation of the pixel embraces both the molecular motion and the convection flow fluctuations,

$$\partial\mathbf{v}(\mathbf{r})=\partial\mathbf{v}_m(\mathbf{r})+\partial\mathbf{v}_C(\mathbf{r}). \tag{5}$$

Whenever one can neglect the mutual correlation between the flow and the molecular motion, the contribution of both to the spin-echo attenuation can be divided. For Brownian diffusion the velocity correlation time is short compared to the interval of acquisition $\tau_{mc}\ll\tau$, allowing us to assume the velocity fluctuation along the applied magnetic field gradient as $\langle\partial\mathbf{v}_{mg}(t)\partial\mathbf{v}_{mg}(0)\rangle=2D\delta(t)$. This provides the spin-echo attenuation from Eq. (3) as

$$\beta_m(\mathbf{r},\tau)=D\int_0^\tau \mathbf{F}^2(\mathbf{r},t)dt \tag{6}$$

with D being the self-diffusion constant. The attenuation β_m does not depend on the position of the pixel $\mathbf{r}$, if a uniform gradient is applied to a homogeneous sample. For slow velocity variations of nonstationary convection with respect to the duration of the acquisition $\tau_{Cc}\gg\tau$, the resulting attenuation follows from Eq. (4) and the definition of the phase Eq. (2):

$$\beta_C(\mathbf{r})=\frac{1}{2N^2}\sum_m\sum_n\int_0^\tau\int_0^\tau \mathbf{F}(\mathbf{r},m\partial t+t_1)\partial\mathbf{v}_C(\mathbf{r},m\partial t+t_1)\times\partial\mathbf{v}_C(\mathbf{r},n\partial t+t_2)\mathbf{F}(\mathbf{r},n\partial t+t_2)dt_1dt_2. \tag{7}$$

∂t is the time between two successive acquisitions. Since $\mathbf{F}$ is periodic $[\mathbf{F}(m\partial t+t)=\mathbf{F}(t)]$ with the period ∂t and the change of the velocity $\partial\mathbf{v}_C$ during the time of the acquisition is small we can further express the attenuation as

$$\beta_c=\frac{1}{2N^2}\sum_m\sum_n\partial v_g(m\partial t)\partial v_g(n\partial t)\left[\int_0^\tau\mathbf{F}(t)dt\right]^2=\frac{1}{2}\langle\partial v_g^2\rangle_C\left[\int_0^\tau\mathbf{F}(t)dt\right]^2. \tag{8}$$

In the last step we have replaced the sum with an integral $\Sigma\rightarrow\int dt/\partial t$. The projection of the velocity on the direction of the gradient is denoted with the subscript g. Here $\langle\partial v_g^2\rangle_C$ is the mean squared velocity fluctuation of the flow projected on the direction of the magnetic field gradient at the location of the picture element $\mathbf{r}$ and is defined as

$$\langle\partial v_g^2\rangle_C=\frac{1}{N^2}\sum_m\sum_n\partial v_g(m\partial t)\partial v_g(n\partial t)=\frac{1}{t_m^2}\int_0^{t_m}\int_0^{t_m}\partial v_g(t')\partial v_g(t'')dt'dt'', \tag{9}$$

where the time of the measurement is $t_m=N\partial t$. Note that the average is taken over a much longer time t_m (several minutes) in $\langle\cdots\rangle_C$ then in $\langle\cdots\rangle$ (less then a second) average for a single acquisition.

For a usual PGSE sequence with the gradient pulse width δ and the interspacing Δ, the total attenuation of the pixel is

$$\beta(\mathbf{r})=\beta_m(\mathbf{r})+\beta_C(\mathbf{r})$$
$$=(\gamma G(\mathbf{r})\delta)^2 D(\mathbf{r})\left(\Delta-\frac{\delta}{3}\right)+\frac{1}{2}(\gamma G(\mathbf{r})\delta\Delta)^2\langle\partial v_g^2(\mathbf{r})\rangle_C. \tag{10}$$

If the convective velocity field $\mathbf{v}_C$ can be separated into a dimensionless time-dependent part $a(t)$ and a space-dependent part as $\mathbf{v}_C(\mathbf{r},t)=a(t)\mathbf{v}_r(\mathbf{r})$ and if we consider the gradient as the product of its spatial $\mathbf{g}_r$ and temporal g_t part, then the convective attenuation β_C Eq. (7) becomes

$$\beta_C(\mathbf{r})=\frac{\gamma^2}{2N^2}\sum_m\sum_n\int_0^\tau\int_0^\tau\int_0^{m\partial t+t_1} g_t(t')dt'$$
$$\times\mathbf{g}_r(\mathbf{r})\cdot\mathbf{v}_r(\mathbf{r})\partial a(m\partial t+t_1)\partial a(n\partial t+t_2)$$
$$\times\mathbf{v}_r(\mathbf{r})\cdot\mathbf{g}_r(\mathbf{r})\int_0^{n\partial t+t_2} g_t(t'')dt''dt_1dt_2. \tag{11}$$

This lengthy expression simplifies for a PGSE experiment (Fig. 1) into

$$\beta_C(\mathbf{r})=\frac{1}{2}(\gamma\Delta\delta)^2\langle\partial a^2\rangle_C(\mathbf{g}_r(\mathbf{r})\cdot\mathbf{v}_r(\mathbf{r}))^2. \tag{12}$$

Equation (12) shows explicitly the spatial dependence of the attenuation factor. It is given with a projection of the velocity on the magnetic gradient field. The strength of the attenuation, for fixed parameters δ, Δ, τ, and gradient strength, is related to the time variation of the convective velocity. In this way, one can see that the spatial dependence of the attenuation factor β_C is determined by the spatial velocity profile (or vice versa) and the magnitude of β_C reveals the time fluctuations of nonstationary macroscopic flows.

The attenuation of the gradient spin-echo, in addition to the molecular self-diffusion, may comprise the information about fluctuations in nonstationary macroscopic flows. Thus the preparation of measurements and the interpretation of data requires all due precaution.

The approach to the evaluation of the effect of a nonstationary flow on the spin-echo is equivalent to the one used in the study of granular flow made by Seymour *et al.* [9].

Now our goal is to find the velocity profile and the time variation of its magnitude for the natural convection in a horizontal cylinder in order to estimate its effect on the spin-echo attenuation. To do so, we have to solve a nonlinear system of equations and simplify it to the lowest possible terms to get the Lorenz system of equations.

III. FREE CONVECTION

The three equations describing incompressible fluid in gravity force field **g**, are Navier-Stokes equation, heat conduction equation, and continuity equation [20]:

$$\frac{\partial\mathbf{v}}{\partial t}+(\mathbf{v}\cdot\boldsymbol{\nabla})\mathbf{v}=-\frac{1}{\rho}\nabla p+\nu\nabla^2\mathbf{v}+\mathbf{g}, \tag{13a}$$

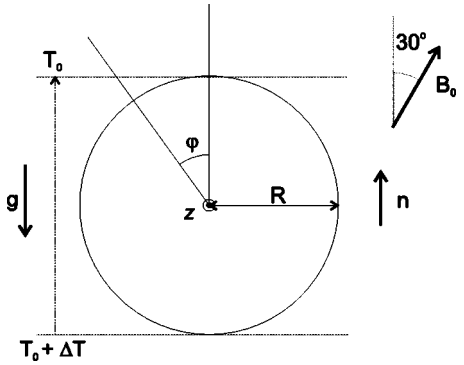

FIG. 2. The geometry of the sample: z axis is perpendicular to the plane of the paper and coincides with the symmetry axis of the cylinder. The vertical axis x (unit vector **n**) is antiparallel to gravitational acceleration. The temperature at the bottom of the circumference is ΔT higher than the temperature T_0 at the top and is assumed to fall linearly from the bottom to the top. B_0 denotes earth's magnetic field, which is on site inclined by 30° from the vertical.

$$\frac{\partial T}{\partial t}+\mathbf{v}\cdot\boldsymbol{\nabla}T=\chi\nabla^2T, \tag{13b}$$

$$\boldsymbol{\nabla}\cdot\mathbf{v}=0. \tag{13c}$$

Here **v**, **g**, p, T, ρ, ν, and χ are, respectively, velocity profile, gravitational acceleration, pressure, temperature, density, kinematic-viscosity, and thermometric-conductivity (or thermal diffusivity) of the liquid.

In what follows, the fluid is assumed incompressible and we will make the Boussinesq approximation [25]—the only temperature-dependent quantity is density:

$$\rho=\rho_0(1-\beta T'). \tag{14}$$

Here ρ_0 is the density of the liquid at the point where the temperature is T_0, β is thermal-expansion coefficient $\beta=-(1/\rho)\partial\rho/\partial T$, and T' is the temperature deviation from T_0. The pressure p is

$$p=\rho_0\mathbf{g}\cdot\mathbf{r}+p'+\text{const} \tag{15}$$

and p' is considered small. The first term on the right side of Eq. (13a) can be written to the first order as

$$\frac{\nabla p}{\rho}=\mathbf{g}+\frac{\nabla p'}{\rho_0}+\mathbf{g}T'\beta \tag{16}$$

and thus Eq. (13a) becomes

$$\frac{\partial\mathbf{v}}{\partial t}+(\mathbf{v}\cdot\boldsymbol{\nabla})\mathbf{v}=-\nabla\left(\frac{p'}{\rho}\right)+\nu\nabla^2\mathbf{v}-\beta T'\mathbf{g}. \tag{17}$$

We will describe the convection in a horizontally oriented cylinder with the diameter $d=2R$. The geometry is shown in Fig. 2. In accordance with Lorenz derivation and to simplify the calculations, it is assumed that the system is translationally invariant along the symmetry axis of the cylinder (denoted in Fig. 2 by z), so that convection rolls extend to infinity. The temperature at the edge of the cylinder is as-

sumed to fall linearly from the bottom to the top of the circumference and, written in cylindrical coordinates, is

$$T(r,\varphi,t)=T_0+\frac{1}{2}\Delta T\left(1-\frac{r}{R}\cos\varphi\right). \tag{18}$$

ΔT is the temperature difference between the bottom and the top of the cylinder (Fig. 2).

The continuity equation (13c) is automatically fulfilled, if we introduce a stream function ψ such that

$$v_r=-\frac{1}{r}\frac{\partial\psi}{\partial\varphi},\quad v_\varphi=\frac{\partial\psi}{\partial r}. \tag{19}$$

In the next step we introduce the deviation $\theta(r,\varphi,t)$ from the linear temperature profile via

$$T(r,\varphi,t)=T_0+\frac{1}{2}\Delta T\left(1-\frac{\mathbf{r}\cdot\mathbf{n}}{R}\right)+\theta(r,\varphi,t). \tag{20}$$

Here **n** denotes a unit vector antiparallel to the direction of gravitational acceleration and signifies the axis from which the polar angle φ is measured.

We get rid of the pressure term in the Navier-Stokes equation by applying the curl to both sides of the equation. Further, we replace the velocity and the temperature field by Eqs. (19) and (20), and we get the equations

$$\frac{\partial\theta}{\partial t}=-\frac{1}{r}\frac{\partial(\psi,\theta)}{\partial(r,\varphi)}+\chi\nabla^2\theta+\frac{\Delta T}{2R}\left(-\frac{\partial\psi}{\partial r}\sin\varphi-\frac{1}{r}\frac{\partial\psi}{\partial\varphi}\cos\varphi\right), \tag{21}$$

$$\frac{\partial\nabla^2\psi}{\partial t}=-\frac{1}{r}\frac{\partial(\psi,\nabla^2\psi)}{\partial(r,\varphi)}+\nu\nabla^2(\nabla^2\psi)+g\beta\left(-\frac{\partial\theta}{\partial r}\sin\varphi-\frac{1}{r}\frac{\partial\theta}{\partial\varphi}\cos\varphi\right), \tag{22}$$

with the notation $\partial(a,b)/\partial(r,\varphi)=(\partial a/\partial r)(\partial b/\partial\varphi)-(\partial a/\partial\varphi)(\partial b/\partial r)$.

In order to simplify this system of equations, we impose a free boundary condition for the velocity and assume a left-right symmetry for the velocity profile

$$\left.\frac{\partial\psi}{\partial\varphi}\right|_R=0,\quad \psi(r<R)<\infty,$$
$$\psi(-\varphi)=-\psi(\varphi),\quad \psi(\varphi+\text{integer}\times 2\pi)=\psi(\varphi). \tag{23}$$

By assuming a free boundary condition, we limit ourselves to the space outside some boundary layer [20]. The thickness of the layer is approximately given by $h\sim\sqrt{\nu l/v_0}$, where v_0 is the velocity outside the layer and l is its length. Following the definition of θ, the quantity is zero at the boundary and the angle symmetry is obvious for the presumed velocity symmetry:

$$\theta(R,\varphi,t)=0,\quad \theta(r<R)<\infty,$$
$$\theta(-\varphi)=\theta(\varphi),\quad \theta(\varphi+\text{integer}\times 2\pi)=\theta(\varphi). \tag{24}$$

Equations (21) and (22), with boundary conditions Eqs. (23) and (24) can be solved with a series expansion in a suitable orthonormal system—in this case the product of cylindrical Bessel and harmonical functions:

$$\psi(r,\varphi,t)=\chi\sum_{nm}a_{nm}(t)J_n(\xi_{nm}r/R)\sin n\varphi, \tag{25}$$

where ξ_{nm} is the mth zero of the nth Bessel function J_n. Likewise, we can write down the temperature deviation as

$$\theta(r,\varphi,t)=\frac{\Delta T}{R_y}\sum_{nm}b_{nm}(t)J_n(\xi_{nm}r/R)\cos n\varphi. \tag{26}$$

The coefficients in the series expansion are

$$a_{nm}(t)=\frac{2}{\chi\pi\dot{J}_n^2(\xi_{nm})}\times\int_{-\pi}^{\pi}d\varphi\int_0^R drr\psi(r,\varphi,t)J_n(\xi_{nm}r/R)\sin n\varphi \tag{27}$$

and

$$b_{nm}(t)=\frac{R_y}{\Delta T\pi\dot{J}_n^2(\xi_{nm})}\times\int_{-\pi}^{\pi}d\varphi\int_0^R drr\theta(r,\varphi,t)J_n(\xi_{nm}r/R)\cos n\varphi. \tag{28}$$

Since we are interested only in the first approximation of motion, we choose to keep only the first terms in the series expansion:

$$\psi(r,\varphi,t)=\chi a_{11}(t)J_1(\xi_{11}r/R)\sin\varphi, \tag{29}$$

$$\frac{R_y}{\Delta T}\theta(r,\varphi,t)=b_{02}(t)J_0(\xi_{02}r/R)+b_{11}(t)J_1(\xi_{11}r/R)\cos\varphi. \tag{30}$$

R_y is a control parameter known as the Rayleigh number:

$$R_y=\frac{\beta g\Delta T d^3}{\nu\chi}. \tag{31}$$

The term with $J_0(\xi_{01}r/R)$ is omitted because of the definition of temperature deviation (the average should be zero). If we would choose to keep more terms in the expansion of ψ, a realistic no-slip boundary condition could be satisfied, but the solution is then too complicated to be physically tractable and even the approximations made (longitudinal symmetry, Bousinesq approximation, and boundary temperature profile) are then questionable. By numerically solving the equations and comparing the solutions it was observed that the solution for the no-slip boundary condition requires more than two terms to be equivalent to the one term free boundary solution with the no-slip boundary condition

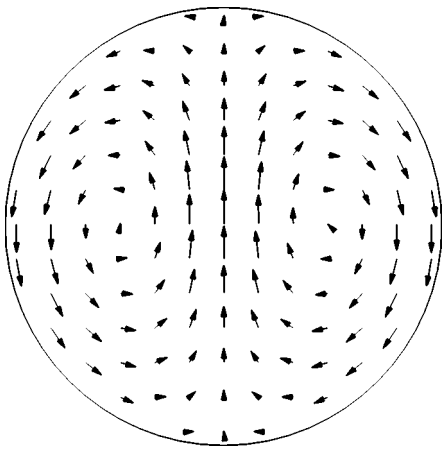

FIG. 3. Velocity profile in the first approximation in a horizontally oriented cylinder heated from below. In this particular image, fluid is rising in the middle and descending at the edge. With a free boundary condition, the velocity at the boundary remains finite whereas in a real case it vanishes.

accounted for with a boundary layer. So complicated solutions are outside the scope of this work especially because the first-order approximation gives the solution of a correct order.

With the expressions for the stream function and temperature deviation [Eqs. (29) and (30)] we get a nonlinear Lorenz system of equations:

$$b_{02}'=c_2a_{11}b_{11}-\xi_{02}^2b_{02}-R_yc_1a_{11}, \tag{32a}$$

$$b_{11}'=-c_3a_{11}b_{02}-\xi_{11}^2b_{11}, \tag{32b}$$

$$a_{11}'=-\sigma\xi_{11}^2a_{11}-\sigma c_4b_{02}, \tag{32c}$$

where the prime denotes the derivative with respect to the normalized time $\vartheta=(\chi/R^2)t$. Dimensionless parameter $\sigma=\nu/\chi$, and numerical constants are

$$c_1=\frac{\xi_{11}\int_0^1 J_0(\xi_{11}x)J_0(\xi_{02}x)xdx}{4\int_0^1 J_0^2(\xi_{02}x)xdx}\approx 0.80,$$

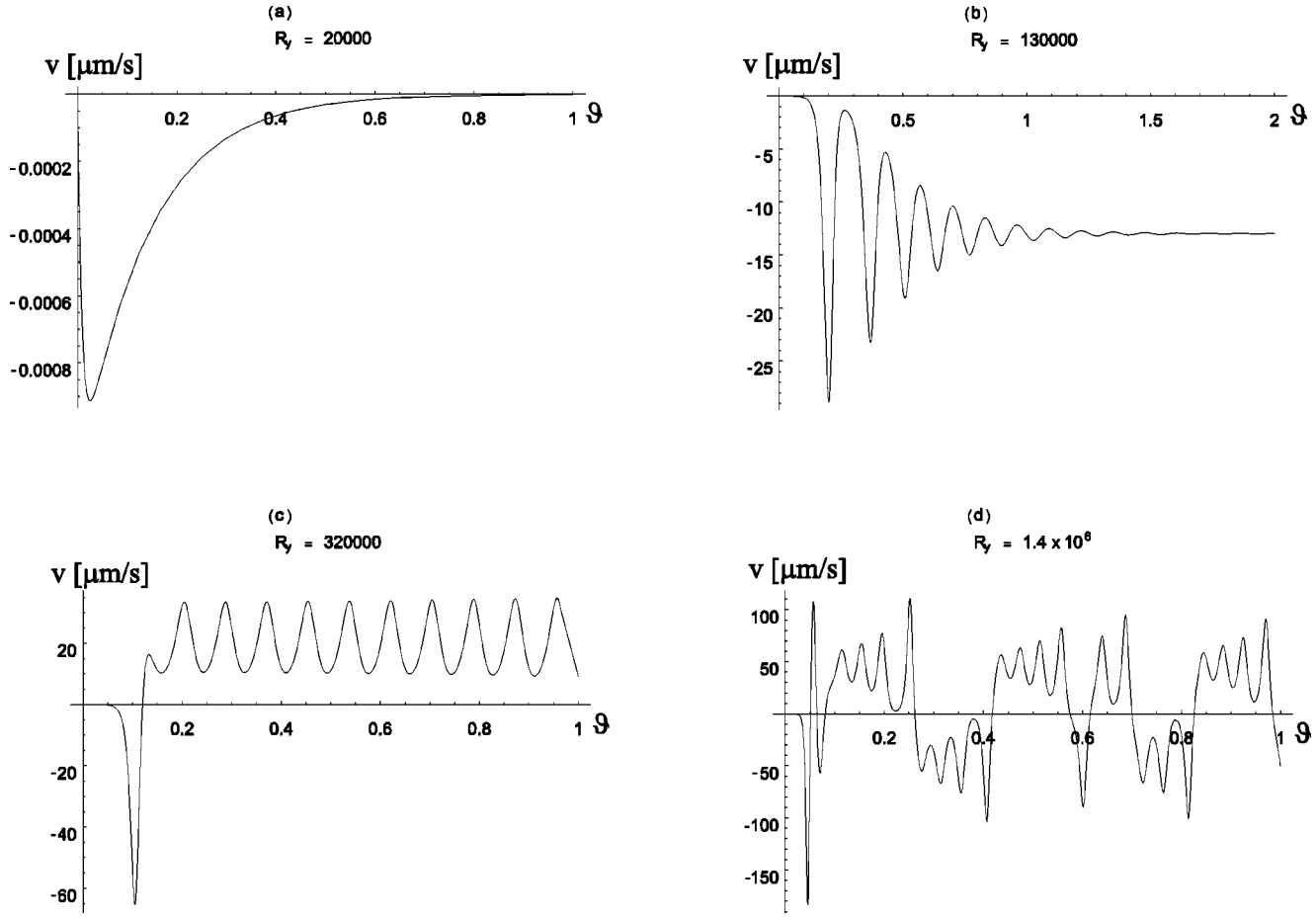

FIG. 4. Amplitude of velocity a_{11} as a function of normalized time τ for some arbitrary initial condition (in this case $a_{11}=0, b_{11}=0, b_{02}=1$) and for different values of control parameter R_y. The value $a_{11}=1$ corresponds to the velocity $v=1\times10^{-6}$ m/s at the center of the cylinder and $\vartheta=1$ corresponds to 3.5×10^4 s. (a) Small R_y corresponds to small temperature difference ΔT. The liquid is stable and no convection occurs. The only heat transfer is through heat conduction. (b) For values of R_y larger than 2.5×10^4, natural convection arises. The flow becomes stationary after a few oscillations. (c) With R_y approaching the value 3.1×10^5, the oscillations become less and less dampened until they finally escalate and the motion becomes chaotic. (d) Chaotic natural convection. For control parameter shown, the changes in a_{11} are on the order of 10^2 in normalized time span of the order 10^{-3}. The temperature difference in this case is $\Delta T=0.01$ K.

$$c_2=\frac{\xi_{11}\int_0^1 J_1'(\xi_{11}x)J_1(\xi_{11}x)J_0(\xi_{02}x)dx}{2\int_0^1 J_0^2(\xi_{02}x)xdx}\approx 2.6,$$

$$c_3=\xi_{02}\frac{\int_0^1 J_1(\xi_{02}x)J_1(\xi_{11}x)J_1(\xi_{11}x)dx}{\int_0^1 J_1^2(\xi_{11}x)xdx}\approx 3.8,$$

$$c_4=\frac{\xi_{02}\int_0^1 J_1(\xi_{02}x)J_1(\xi_{11}x)xdx}{8\xi_{11}^2\int_0^1 J_1^2(\xi_{11}x)xdx}\approx 0.019.$$

The quantity of interest is the velocity associated with a_{11}. The liquid studied here is water at 20 °C with $\sigma=6.3$, $\chi=1.4\times10^{-7}$ m^2/s, $\nu=9\times10^{-7}$ m^2/s, and $\beta=2.2\times10^{-4}$/K. In this case it follows that the value $a_{11}=1$ corresponds to the velocity $v=1\times10^{-6}$ m/s at the center of the cylinder. The value $\vartheta=1$ gives time $t=3.5\times10^4$ s. The system [Eqs. (32)] was solved numerically with a nonstiff implicit Adams algorithm with order between 1 and 12 or stiff Gear backward difference formula method with order between 1 and 5 depending on the convergence of the solutions [26]. The velocity profile is shown in Fig. 3 and the amplitude of the velocity in the center of the cylinder, for different values of control parameter R_y, is shown in Fig. 4. One can see in Fig. 4(a) that for small values of R_y the liquid is stable and no convection occurs. For Rayleigh numbers larger than 2.5×10^4 the convection appears that becomes stationary after a while [Fig. 4(b)]. Only at even greater values of the control parameter [$R_y=3.1\times10^5$, Fig. 4(c)] the convection becomes chaotic, yet the period is somewhat fixed and varies with R_y. A deeper understanding of the nature of bifurcations can be found in Ref. [27].

IV. EXPERIMENT

The experiment is described in details in Ref. [10]. It is a basic PGSE experiment combined with spin-warp imaging to reveal the space distribution of the self-diffusion constant of water in a 0.2-m-diameter tube. The scheme for magnetic fields of a single frame in the experiment is shown in Fig. 5. The acquisition in one frame of the measurement takes approximately 0.5 s and is repeated after 6 s. The magnetization field is needed because the experiment is performed in a relatively weak earth's magnetic field. The magnetization is turned on for 3 s to allow a sufficient relaxation time. The idle time of 3.5 s in the frame is required because of the duty cycle of the magnetization amplifier. The probe is inside a receiving coil with its diameter 1 cm larger than the sample cylinder. The symmetry axes of the probe and the receiver coil are parallel and perpendicular to the magnetic field. The cylinder is touching the coil at the bottom with an air gap on the top. The probe is neither isolated nor thermally stabilized. The magnetization coil can heat up to 50 °C, depending on the external condition (air temperature, draft). As our model and the following discussion show, even a small temperature variation can induce thermal convection. The condition that the convection be absent for water is about one degree per 6.7 km [20]. As mentioned before, velocity fluctuations induced by convection cause additional attenuation of the signal from each picture element comprising the image. The magnetic field gradient used in the experiment was of the form

$$\mathbf{g}_r=\nabla|((Gz+B_0)\cos 30°,(Gz+B_0)\sin 30°,$$

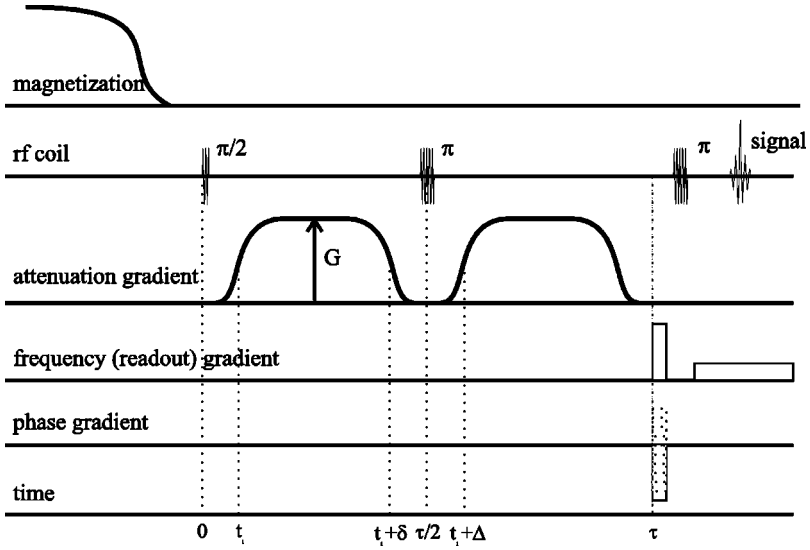

FIG. 5. Magnetic fields in PGSE measurement of self-diffusion. The distribution of diffusivity is examined with a spin-warp 2D imaging technique. The magnetization field magnitizes the sample, thus enhancing the signal. The rf field first excites spins with a $\pi/2$ pulse and then inverts their phase at time $\tau/2$ as is customary in PGSE. π pulse is also a part of the spin-warp imaging sequence. The attenuation gradient causes the attenuation of the spin echo and is in our case perpendicular to the phase and read gradients of the spin-warp imaging sequence. The phase and read gradients produce a 2D image of a projection of distribution of spins on a plane perpendicular to the cylinder symmetry axis. The time axis indicates the time of the spin echo τ, length of gradient pulses δ, and their separation Δ. Times are shown in appropriate ratio. The time δ used in our measurements was varied between 0 and 300 ms.

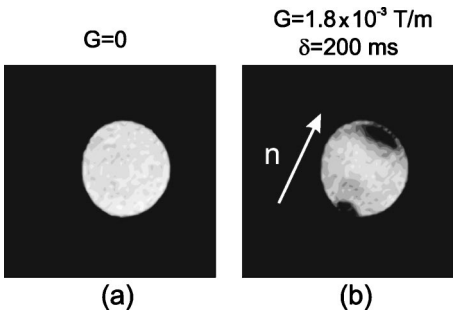

FIG. 6. PGSE MR image of a cross section of a cylinder, showing the space distribution of self-diffusion constant. (a) Image of spin density with G set to zero. (b) Image of diffusivity with gradient pulses of δ length and strength of $G=1.8\times10^{-3}$ T/m. The patches at the top and the bottom of the cross section are caused by natural convection.

$$G(x\cos 30° - y\sin 30°))|, \tag{33}$$

with the amplitude $G=1.8\times10^{-3}$ T/m. At a first glimpse, the expression for the gradient field may appear a bit complicated. This is because the field is of quadrupolar form and aligned along the direction of earth's magnetic field, which is inclined by 30° from the vertical axis **n**. The direction of the earth's magnetic field also defines the vertical axis of MR images shown here.

A series of images was taken for different lengths δ of gradient pulses (Fig. 6). One can observe that, aside from the uniform attenuation brought about by self-diffusion, there is also additional attenuation in the form of dark patches. We can explain these patches with the convection pattern given by Eq. (19), evaluated with the stream function of Eq. (29) and a boundary layer accounted with $(1-e^{-(1-r/R)h/R})$, and the attenuation form of Eq. (10). The boundary layer thickness is h and the velocity near the wall falls to zero linearly with the distance from the wall. Figure 7 shows the MR

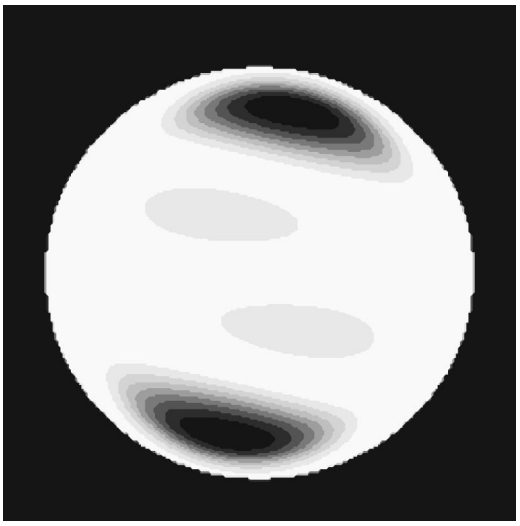

FIG. 7. Attenuation caused by convection. Shown is the exponent of the square of the scalar product of gradient field and velocity field [given in Eq. (12)] for variance of velocity fluctuation given by Eq. (34). The velocity field of Eq. (19) is modified in such a way that velocity vanishes at the boundary.

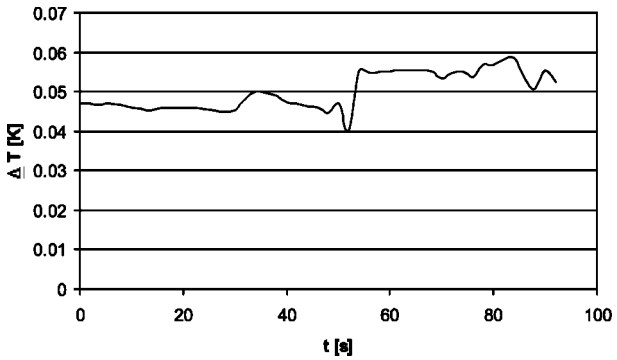

FIG. 8. The time diagram of the temperature difference ΔT between the bottom and the top of the cylinder circumference.

image predicted with this velocity field ($h=1$ cm) and with the same parameters as were used in the experiment.

According to Eq. (4), we infer from the attenuation of pixels on the MR image (Fig. 6) that the velocity changes between different frames should be on the order of

$$\partial v_C \approx \frac{3}{\gamma\Delta\,\delta G 0.5} \approx 0.1 \text{ mm/s}, \tag{34}$$

where two adjacent frames are separated by ∂t. The factor 0.5 is the product of maximal value of $J_1(\xi_{11}x)$ and $\cos 30°$; in our case the repetition time $\partial t=6s$. This corresponds to the normalized time span of $\partial\vartheta=1\times10^{-4}$. The velocity fluctuations of 0.1 mm/s signify the variation of $\partial a_{11}=1\times10^2$. Such velocity fluctuations are represented in Fig. 4(d), which corresponds to a Rayleigh number of 1.4×10^6. In our case this means a temperature difference $\Delta T=0.02\pm0.01$ K.

The temperature difference between the bottom and the top of the circumference was also measured with an array of thermocouples. The time diagram of ΔT is shown in Fig. 8. The temperature difference fluctuates by 0.01 K around the average of 0.05 K on a time scale of a few seconds with occasional jumps that are not correlated with the measurement but should be contributed to the external disturbances. The temperature is measured on the outer side of the cylinder walls. We estimate that the temperature inside the cylinder is only slightly smaller (a few percent) since the walls are thin (less than 1 mm).

V. CONCLUSION

The measurements of the self-diffusion constant with NMR PGSE, although well-established, still need to be evaluated cautiously. If we would not make an image of the sample we would not be able to see the effect of natural convection and we would misleadingly overestimate the self-diffusion constant of the liquid. However, the effect, under the conditions described herein, is not very strong and is observable only in the limit of strong and long gradient pulses. In fact, the flow is so slow that the measurement of the velocity with NMR is virtually impossible. To get a measurable signal dephasing from the convective flow, a strong gradient needs to be applied for a long time (compared to relaxation). The signal of such measurement

is so noisy that averaging is needed. But, when the flow is not steady, the averaging additionally attenuates the signal, which could be misinterpreted as an enhanced self-diffusion.

Of course the above given calculations are only the crudest estimation of what takes place in the probe. Also, thermal takenboundary conditions are not as well-defined as were here to be. The fact that the measured temperature difference is somewhat higher than predicted is understandable since the prediction is based on the convection with the free boundary conditions. This work should not be understood as a new technique of measuring the Rayleigh number but as a demonstration of the influence of a nonsteady flow on the averaging of the spin-echo signal.

[1] P.T. Callaghan, *Principles of Nuclear Magnetic Resonance Microscopy* (Oxford University Press, Oxford, 1991).

[2] N. Blombergen, E.M. Purcell, and R.V. Pound, Phys. Rev. **73**, 679 (1948).

[3] H.C. Torrey, Phys. Rev. **104**, 563 (1956).

[4] H.Y. Carr and E.M. Purcell, Phys. Rev. **94**, 630 (1954).

[5] E.L. Hahn, Phys. Rev. **80**, 580 (1950).

[6] E.O. Stejskal, J. Chem. Phys. **43**, 3597 (1965); E.O. Stejskal and J.E. Tanner, *ibid.* **42**, 288 (1965).

[7] P. Stilbs, Prog. Nucl. Magn. Reson. Spectrosc. **19**, 1 (1987).

[8] J. Stepišnik, Prog. Nucl. Magn. Reson. Spectrosc. **17**, 187 (1985); J. Stepišnik, Physica B **198**, 299 (1994); J. Stepišnik, M. Kos, G. Planinšič, and V. Eržen, J. Magn. Reson., Ser. A **107**, 167 (1994); J. Stepisnik, Z. Phys. Chem. (Munich) **190**, 51 (1995).

[9] J.D. Seymour, A. Caprihan, S.A. Altobelli, and E. Fukushima, Phys. Rev. Lett. **84**, 266 (2000).

[10] A. Mohorič, J. Stepišnik, M. Kos, and G. Planinšič, J. Magn. Reson. **136**, 22 (1999).

[11] D.O. Kuethe, Phys. Rev. A **40**, 4542 (1989); D.O. Kuethe and J.H. Gao, Phys. Rev. E **51**, 3252 (1995).

[12] B. Manz, J.D. Seymour, and P.T. Callaghan, J. Magn. Reson. **125**, 153 (1997).

[13] W.J. Goux, L.A. Verkruyse, and S.J. Salter, J. Magn. Reson. **88**, 609 (1990).

[14] N. Hedin and I. Furó, Geomagn. Aeron. **131**, 126 (1998).

[15] J. Lounila, K. Oikarinen, P. Ingman, and J. Jokisaari, J. Magn. Reson, Ser. A **118**, 50 (1996).

[16] J. Weis, R. Kimmich, and H.P. Müller, Magn. Reson. Imaging **14**, 319 (1996).

[17] S.J. Gibbs, T.A. Carpenter, and L.D. Hall, J. Magn. Reson., Ser. A **105**, 209 (1993).

[18] H. Bénard, Rev. Gen. Sci. Pures Appl. **11**, 1261 (1900); **11**, 1309 (1900); Ann. Chim. Phys. **23**, 62 (1901).

[19] Lord Rayleigh, Philos. Mag. **32**, 529 (1916).

[20] L.D. Landau and E.M. Lifshitz, *Fluid Mechanics* (Pergamon, Oxford, 1987).

[21] C. Normand and Y. Pomeau, Rev. Mod. Phys. **49**, 581 (1977).

[22] G.S. Charlson and R.L. Sani, Int. J. Heat Mass Transf. **13**, 1479 (1970); **14**, 2157 (1971).

[23] E.N. Lorentz, J. Atmos. Sci. **20**, 130 (1963).

[24] B. Saltzman, J. Atmos. Sci. **19**, 329 (1962).

[25] J. Boussinesq, *Theorie Analytique de la Chaleur* (Gauther-Villars, Paris, 1903), Vol. 2, p. 172.

[26] W.H. Press, B.P. Flannery, S.A. Teukolsky, and W.T. Vetterling, *Numerical Recipes* (Cambridge University Press, Cambridge, 1986).

[27] C. Sparrow, *The Lorenz Equations, Bifurkations, Chaos, and Strange Attractors* (Springer-Verlag, New York, 1982).